Microporous and Mesoporous Materials 132 (2010) 163–173

Contents lists available at ScienceDirect

Microporous and Mesoporous Materials

journal homepage: www.elsevier.com/locate/micromeso

Synthesis of mesoporous amorphous silica by Kr and Xe ion implantation: Transmission electron microscopy study of induced nanostructures

E. Oliviero [a,*], M.-O. Ruault [a], B. Décamps [a], F. Fotuna [a], E. Ntsoenzok [b], O. Kaïtasov [a], S. Collin [a]

[a] CSNSM, UMR 8609, CNRS/IN2P3-Univ-Paris-Sud, Bâtiment 108, 91405 Orsay Campus, France
[b] CEMHTI-CNRS, 3A, rue de la férollerie, 45071 Orléans, France

ARTICLE INFO

Article history:
Received 13 November 2009
Received in revised form 18 February 2010
Accepted 20 February 2010
Available online 24 February 2010

Keywords:
Mesoporous silica
Noble gas implantation
Bubbles
Cavities
Structural investigation

ABSTRACT

Thermally grown amorphous SiO_2 was implanted at room temperature with heavy noble gases Kr and Xe in order to create cavities in the oxide and increase its porosity. The implantation energies were chosen in order to have the same implantation depth for both ions. Although both ions induce bubbles in amorphous SiO_2, bubble size and spatial distribution depend upon the ion mass. Moreover, Xe implantation leads to the additional formation of "nanoclusters". Thermal stability of bubbles/cavities depends on the implanted ion. The nucleation of bubbles and nanoclusters in amorphous SiO_2 is discussed in terms of ion mobility, gas–defect interactions, and chemical interaction. Bubble growth is shown to occur by a migration and coalescence process.

1. Introduction

With the constant miniaturization of electronic devices and consequently the continual increase in the density of multilevel interconnections, material with lower dielectric constant (k) value is required to overcome some of the resulting problems such as transmission delay, power consumption and cross-talk noise. Until now, SiO_2 having a dielectric constant of 3.9 has been used as a dielectric material for the interconnections in integrated circuit devices. The International Technology Roadmap for Semiconductors (ITRS) has projected that the dielectric constant of the material should fall below 2 by 2010. There are two possible approaches to achieve this. The obvious one is the use of new materials with lower k, but care has to be taken on their compatibility with microelectronics (interface with silicon, mechanical strength, thermal and etching properties, etc.). The second approach is to decrease the effective dielectric constant of SiO_2. This can be achieved by incorporating pores into the material. Air has a dielectric constant of roughly 1.00059, thus increasing the SiO_2 layer porosity leads to the reduction of the dielectric constant. The pore structure and its distribution have distinct influences on the basic physical properties of the material. While the reduction in k is desirable, there are also adverse effects such as deterioration of the mechanical properties as porosity increases. There is also the problem of moisture adsorption in the presence of pores at the surface. Therefore, an ideal porous material would consist of a network of small pores embedded into material, with a regular size distribution (uniformly-sized and distributed pores). An appropriate technique to realize such a pores network within SiO_2 is rare gas ion implantation.

The formation of bubbles/cavities resulting from the agglomeration of noble gas after ion implantation has been extensively studied over several decades in crystalline materials such as metals. Blistering, swelling and embrittlement are unwanted effects in these materials, which are used in fusion or fission reactors [1]. Bubble/cavity formation, blistering and swelling were also studied in semiconductors as smart tools for applications such as impurity gettering [2], strain relaxation [3], thin layer separation [4] and defect engineering [5]. Bubble formation and growth in such materials is a complex phenomenon involving point defect production/recombination, mobility and agglomeration. Because of their extremely low solubility, noble gases have a strong tendency to segregate into gas–vacancy complexes which may further coarsen and grow forming stable gas-filled cavities. The final defect morphology resulting from noble gas implantation and post-annealing is intricate. It consists of point and extended defects of both vacancy and interstitial types. The vacancy-type defects may contain gas. The main factors influencing the eventual defect morphology depends on the rate at which damage is introduced, the thermal and radiation-enhanced mobility of both gas and defects, and most importantly the ability of the gas to permeate from cavities back into the matrix.

* Corresponding author.
E-mail address: oliviero@csnsm.in2p3.fr (E. Oliviero).

1387-1811/$ - see front matter © 2010 Elsevier Inc. All rights reserved.
doi:10.1016/j.micromeso.2010.02.015

The extension of these studies from crystalline to amorphous materials such as SiO_2 could give insights into the damage accumulation processes and a better understanding of the bubble formation mechanisms. Indeed, the formation and growth mechanisms of cavities are relatively well understood in metals [6] and semiconductors [7]. In the case of SiO_2, the nucleation and growth mechanisms of metallic/semiconductor nanoprecipitates has been extensively studied but these mechanisms are not yet well understood for bubbles/cavities [8,9] and require detailed analyses of bubble characteristics including (i) the diffusivity of the gas atoms in SiO_2 and (ii) the nature of defects created by implantation.

The aim of the work presented in this paper is to understand the processes that could play a role in the nucleation and growth of the bubbles formed by Kr or Xe implantation in amorphous SiO_2 (a-SiO_2). Thus, a detailed TEM study of the induced nanostructures (involving bubbles) was performed after two implantation fluences (3.5 and 5×10^{16}/cm^2) and after isochronal annealing up to 1370 K. The as-implanted results are discussed in terms of gas mobility and the interaction between gas atoms and vacancy-type defects or negatively charged defects. The structural evolutions during annealing are explained using the migration and coalescence mechanism.

2. Experimental details

Thermal amorphous SiO_2 layers were grown by heating n-type silicon wafers at 1370 K in ambient air. Samples of two different layer thicknesses (220 nm and 2.3 μm) were used in this study. The samples were implanted, at room temperature, with 220 keV Kr ions or 300 keV Xe ions at the same fluences (3.5 and 5×10^{16} ions/cm^2). The implantation energies were chosen, according to SRIM (Stopping and Range of Ions in Matter) simulations [10], in order to have the same projected range (R_p) of ~120 nm for both ions. Ion flux was kept as low as 1–1.5×10^{12} ion/cm^2 s to avoid any temperature increase during implantation. After implantation, samples were annealed at temperatures ranging from 670 to 1370 K for 1 h under nitrogen atmosphere. The as-implanted and post-annealed samples were characterised by cross-sectional transmission electron microscopy (XTEM) and compared with the ion distributions obtained previously [9] by Rutherford Backscattering Spectrometry (RBS) in specimens implanted under the same experimental conditions. The measurements were performed using a FEI CM12 TEM and a Tecnai G^2 20 TEM. The cross-section samples for XTEM were mechanically thinned by means of a tripod.

For a better comprehension of the XTEM results, a few preliminary remarks are needed before a detailed presentation of the results.

(1) *Amorphization of the Si substrate* occurs when implanting in the 220 nm thick SiO_2 layer. In fact, the ion range is up to about 250 nm for both implanted ions. Thus, a Si band just behind the interface is amorphized due to the induced mixing phenomena at the SiO_2/Si interface and to the induced irradiation defects. During post-annealing $\geqslant$800 K, the amorphous band recrystallizes leaving defects such as dislocations or rod-like defects.

(2) The *thickness* of the 220 nm thick SiO_2 layer was controlled before and after implantation by RBS technique. No swelling of the layer due to noble gas implantation was observed in the bulk specimens. However, a widening of the SiO_2 layer was observed by TEM (Fig. 1). This enlargement occurs during the mechanical thinning process and is due to an increase of the SiO_2 ductility. The change in ductility is induced by the implantation/irradiation. In the following, the deformation of the SiO_2 layer will be taken into account.

(3) *For non-spherical nanostructures*, the size will be given as the equivalent diameter for spherical shape having the same area.

(4) The *density depth distribution* of nanostructures is obtained by counting them in 10–20 nm width bands only if the size of these nanostructures is small enough (i.e. at least half of the band width). In our study nanostructure sizes are mostly quite large so that it is not possible to give the bubble density distribution as a function of depth. The same is true for the distribution of the bubble centres as a function of depth. It seems more accurate to evaluate the projected area of the nanostructures. A normalization is done by dividing the results by the total projected area of all the nanostructures present in the layer. It should be noted that, due to the amorphous structure of SiO_2, it is difficult to assess the thickness of the XTEM specimen in the studied zones. In fact, the XTEM specimen thickness can be evaluated only by the electron transparency of the sample (see for example Fig. 1). The accuracy of such an evaluation is not better than 30–50 nm. However, each projected area depth distribution is obtained on a sufficiently small region, so that the sample thickness variation can be estimated at about 20% inside an individual depth distribution.

3. Results

Both Kr and Xe implanted samples clearly show the formation of nanostructures in the implanted region. A detailed description of the observed nanostructures is given in the following.

3.1. Xe implantation

3.1.1. As-implanted

Figs. 2 and 3 show the nanostructures induced in amorphous SiO_2 by 300 keV Xe implantation at room temperature for fluences of 3.5 and 5×10^{16} Xe/cm^2. Two types of nanostructures are observed:

(i) Nanostructures without Fresnel fringes (Fresnel fringes are characteristic of bubbles/cavities [11]). These nanostructures exhibit a black contrast in overfocus conditions, which tends to vanish in the underfocus condition (Fig. 3a–d). These nanostructures could not therefore be identified as bubbles or cavities. From this point on, these nanostructures will be termed as "nanoclusters".

(ii) Nanostructures identified as bubbles, i.e. exhibiting Fresnel fringes at the interface whose contrast reverse from black to white from under to overfocus conditions [11]

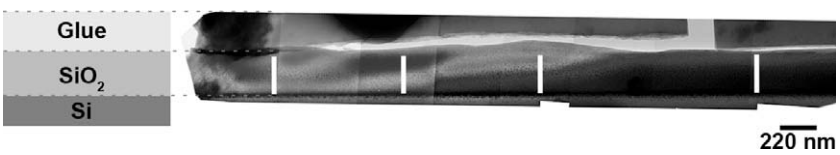

Fig. 1. An assembly of brightfield image showing a TEM cross-section of an as-implanted sample. The white bars illustrate the size of the SiO_2 layer before implantation (220 nm) along the cross-section. The thickness of the TEM sample increases from the left to the right.